Nuclear charge distributions in $1f_{7/2}$-shell nuclei from muonic x-ray measurements

H. D. Wohlfahrt, E. B. Shera, and M. V. Hoehn
Los Alamos Scientific Laboratory, University of California, Los Alamos, New Mexico 87545

Y. Yamazaki* and R. M. Steffen
Department of Physics, Purdue University, Lafayette, Indiana 47907

(Received 14 July 1980)

Precise $2p$-$1s$ muonic x-ray transition energies and energy shifts were measured for the $1f_{7/2}$-shell nuclei ^{39,41}K, ^{40,42,43,44,46,48}Ca, ^{45}Sc, ^{46,47,48,49,50}Ti, ^{51}V, ^{50,52,53,54}Cr, ^{55}Mn, and ^{56}Fe. The data were analyzed in terms of the Barrett moments $\langle r^k e^{-ar} \rangle$ of the nuclear charge distribution, from which equivalent nuclear radii R_k and isotopic and isotonic differences ΔR_k were computed. For those nuclei for which electron-scattering data were available, model-independent rms radii and radius differences were deduced from a combined analysis of the present data and elastic electron-scattering data. The $\Delta N = 2$ isotope shifts between even-A nuclei decrease nearly linearly with increasing N and become negative in the second half ($24 \leq N \leq 28$) of the $1f_{7/2}$ shell; a strong shell-closure effect is evident at $N = 28$. The isotope shifts are independent of Z, suggesting that the added neutrons interact with the entire proton core rather than with the valence protons. The $\Delta Z = 2$ isotone shifts between even-A nuclei decrease smoothly and uniformly with increasing Z for $20 \leq Z \leq 28$ and are essentially independent of N. Like the isotope shifts, the isotone shifts display a sudden increase at $Z = 28$. Both the $\Delta N = 1$ isotope shifts and the $\Delta Z = 1$ isotone shifts show pronounced odd-even staggering. A strong correlation is found between nuclear deformation, as revealed by experimental $B(E2)$ values, and the measured isotope and isotone shifts. The measured isotope and isotone shifts, including those for odd-A nuclei, are satisfactorily described by a simple empirical formula. The experimental results were compared with Hartree-Fock calculations; some recent calculations that include ground-state correlations display improved agreement with experiment through the inclusion of these deformation-related effects.

[NUCLEAR STRUCTURE ^{39,41}K, ^{40,42,43,44,46,48}Ca, ^{45}Sc, ^{46,47,48,49,50}Ti, ^{51}V, ^{50,52,53,54}Cr, ^{55}Mn, ^{56}Fe; measured muonic x-ray spectra; deduced nuclear charge radii, isotope and isotone shifts; performed model-independent combined analysis of muonic x-ray data and elastic electron scattering data; compared charge parameters with Hartree-Fock and other calculations.]

I. INTRODUCTION

Investigation of charge distribution differences for isotones and isotopes provides valuable information about the spatial distribution of valence protons and the polarization of the proton core in response to the addition of protons and neutrons. Recent high-accuracy measurements of charge distribution differences show clearly that the usual empirical mass-radius formulas[1,2] represent only an approximation to the actual variation of nuclear charge radius with mass number. Deviations of the measured charge radii from the empirical mass-radius formulas have been found to follow rather simple trends which are strongly influenced by nuclear shell structure and deformation effects.[3-6] A comparison of these trends with microscopic-model calculations provides a stringent test of the adequacy of the calculations.[3,4,7]

It is known from several experimental[8-12] and theoretical[13-16] investigations of the charge distributions of the doubly closed-shell nuclei ^{40}Ca and ^{48}Ca that a rather complicated polarization of the $Z = 20$ proton core accounts for the fact that the charge radii of these two nuclei are almost exactly the same,[10-12] even though the two nuclei differ by eight neutrons. It was a major goal of the present experiment to determine whether other $1f_{7/2}$ nuclei show effects similar to those observed in the doubly magic Ca isotopes. In addition, the present study represents the first systematic study of isotone shifts and provides an opportunity to compare the core polarization caused by protons and neutrons in the same ($1f_{7/2}$) shell.

In the present paper, muonic-atom charge distribution measurements for all stable isotopes of K, Ca, Sc, Ti, V, Cr, and Mn are reported. These data, together with data of a previous experiment[3] that included, among others, the isotopes of Fe, Co, and Ni, represent all stable $1f_{7/2}$ proton-shell nuclei and most of the $1f_{7/2}$ neutron-shell nuclei (see Fig. 1). In collecting and analyzing the present data, we used procedures similar to those of Ref. 3 so that the two sets of measurements would be as compatible as possible. As a check of the consistency of the two experiments, ^{56}Fe was remeasured in the present work.

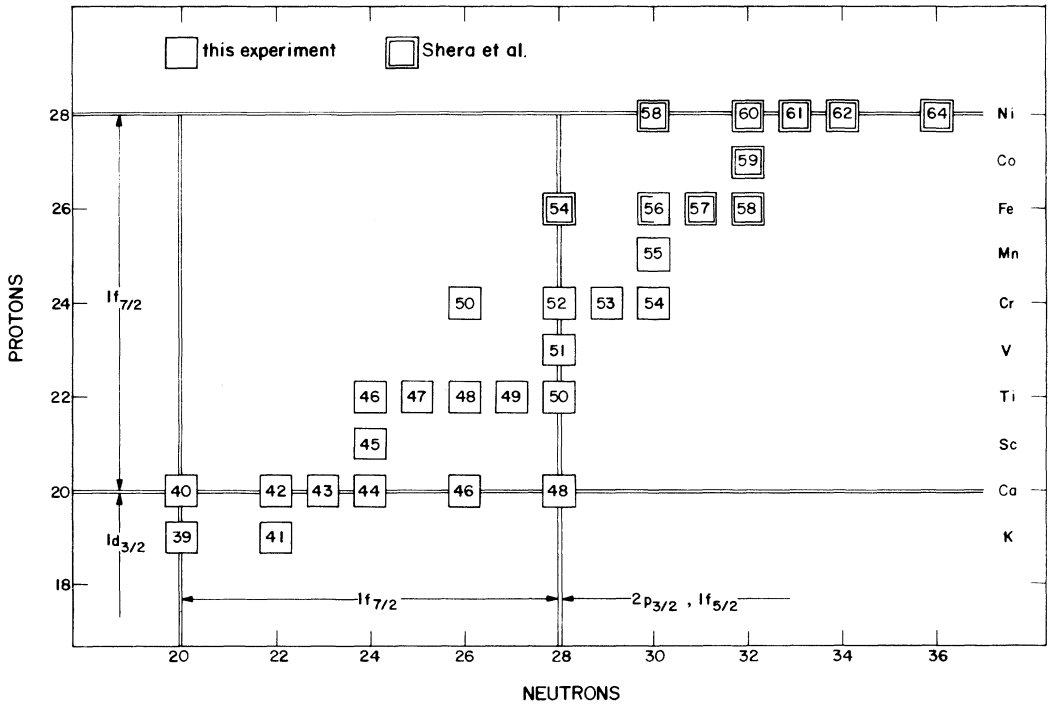

FIG. 1. $1f_{7/2}$ neutron- and proton-shell nuclei investigated by muonic x-ray techniques in the present experiment and in a previous experiment by Shera *et al.* (Ref. 3).

II. EXPERIMENTAL PROCEDURE AND RESULTS

The measurements were carried out at the muon channel of LAMPF. We used the same techniques described in Ref. 3 with minor modifications[17] to accommodate the higher (150 μA) proton beam current and consequent higher muon stopping rates available from LAMPF at the time of the present experiment.

In brief, an arrangement of scintillation counters signaled the stopping of muons in each of three isotopically separated targets. The muonic x rays of each of the three targets and appropriate calibration γ rays were detected with a 60-cm^3 Ge(Li) spectrometer and stored in separate spectra. A total of 21 different nuclei were studied in various combinations of 3. The targets were permuted among the 3 possible target positions to reduce geometric effects. Altogether, 20 separate experimental runs were made during the course of the measurements. The isotopic compositions and the masses of the 21 targets are listed in Table I. The energy-calibration sources listed in Table II provided a sequence of 12 precisely known[18] reference points within the energy range of interest (650 keV–1.4 MeV). Energy calibration data, obtained simultaneously with the x-ray data (that is, during the accelerator beam pulse) and in separate runs following the x-ray measurements, indicated a maximum nonlinearity of the Ge(li) detector and associated electronics of 50 eV. The x-ray energies were corrected for this nonlinearity. The uncertainty of this correction and the absolute error in the calibration energies have been included in the quoted errors of the muonic transition energies.

Figure 2 shows the muonic x-ray spectra, as observed in typical runs, of two isotopes of Ti and of Cr. The shifts in the energies of the x-ray lines are readily apparent. For determination of the muonic x-ray line centroids, the detector response function, a Gaussian convoluted with a low-energy exponential tail, was fitted to the measured spectra with the tail parameters fixed at the values obtained from the calibration lines. The resolution, full width at half maximum, of the detector was approximately 1.8 keV at the energy (932 keV) of the Ti $2p$-$1s$ muonic lines. Since the fine-structure splitting of the $2p$-$1s$ transitions of Ca, Sc, Ti, and V was not resolved, the $2p_{3/2}$-$1s_{1/2}$ and $2p_{1/2}$-$1s_{1/2}$ transition lines were fitted together with the fine-structure splittings fixed at their theoretical values. The uncertainty involved in this fitting procedure was estimated by comparing the $2p_{3/2}$-$1s_{1/2}$ energies obtained from fits with and without a fixed value for the $2p$ fine-structure splitting. The largest difference occurred in the muonic x rays of the K isotopes

TABLE I. Target masses and isotopic compositions. The targets ^{40}Ca, ^{45}Sc, ^{51}V, ^{55}Mn, and ^{56}Fe were of natural isotopic composition and had masses of about 15 g.

Isotope	Target mass (g)	Isotopic composition (%)					
		^{39}K	^{41}K				
^{39}K	10	99.96	0.04				
^{41}K	10	0.82	99.18				
		^{40}Ca	^{42}Ca	^{43}Ca	^{44}Ca	^{46}Ca	^{48}Ca
^{42}Ca	7	5.08	93.65	0.43	0.84	<0.05	<0.05
^{43}Ca	8	10.36	0.80	83.73	5.11	<0.05	<0.05
^{44}Ca	10	1.48	0.04	0.03	98.44	<0.01	<0.01
^{46}Ca	0.08	50.43	0.63	0.17	3.87	43.35	1.56
^{48}Ca	12	5.32	<0.10	<0.10	0.15	<0.10	94.47
		^{46}Ti	^{47}Ti	^{48}Ti	^{49}Ti	^{50}Ti	
^{46}Ti	9	85.90	1.56	10.70	0.84	1.03	
^{47}Ti	11	1.66	82.80	13.90	0.79	0.79	
^{48}Ti	15	0.15	0.30	99.24	0.22	0.10	
^{49}Ti	15	3.48	2.52	24.96	66.36	2.68	
^{50}Ti	2	2.71	2.48	24.10	2.99	67.72	
		^{50}Cr	^{52}Cr	^{53}Cr	^{54}Cr		
^{50}Cr	5	96.80	2.96	0.18	0.04		
^{52}Cr	9	<0.01	99.84	0.14	<0.01		
^{53}Cr	23	0.82	3.37	95.56	0.25		
^{54}Cr	15	0.11	4.01	1.79	94.15		

(15 eV).

The data were also corrected for the presence of the weak muonic x rays from known isotopic impurities and, in the case of odd-A isotopes, for the presence of hyperfine-structure splittings. Neither the isotopic-impurity lines nor the hyperfine (hf) components could be separately resolved because the detector line width was almost twice as large as either the isotope shifts in this mass region or the maximum energy separations of the hf components. The isotope shifts were determined using an iterative procedure in which a multiplet of lines, with intensity ratios fixed according to the known isotopic composition of the targets, was fitted to the measured spectra. Appropriate hf-structure patterns, calculated from the known nuclear magnetic dipole and electric quadrupole moments,[19] were also included in the fitting procedure. When the hf corrections were included, the χ^2 values of the least squares fits improved significantly and the fitted linewidths agreed well with the linewidths of the calibration spectra.

TABLE II. Energy-calibration sources. The listed γ-ray energies are from Ref. 18.

Isotope	γ-ray energy (keV)
^{110}Ag^m	657.762 (2)
	706.682 (3)
	763.944 (3)
	884.685 (3)
	937.493 (4)
	1384.300 (4)
^{182}Ta	1121.301 (5)
	1189.050 (5)
	1221.408 (5)
	1231.016 (4)
^{60}Co	1173.237 (4)
	1332.501 (5)

A weighted least squares adjustment technique, described in Ref. 3, was used to determine a set of "best values" for the $2p_{3/2}$-$1s_{1/2}$ energy differences. The results are given in Table III. For this least squares adjustment the χ^2 per degree of freedom was 0.97, indicating that the energy shift values from all 20 runs were consistent within the statistical errors of a single measurement. The errors for the isotope shifts listed in Table III include only the statistical errors of the measurements; other errors cancel in these energy differences. The errors for all other shifts in-

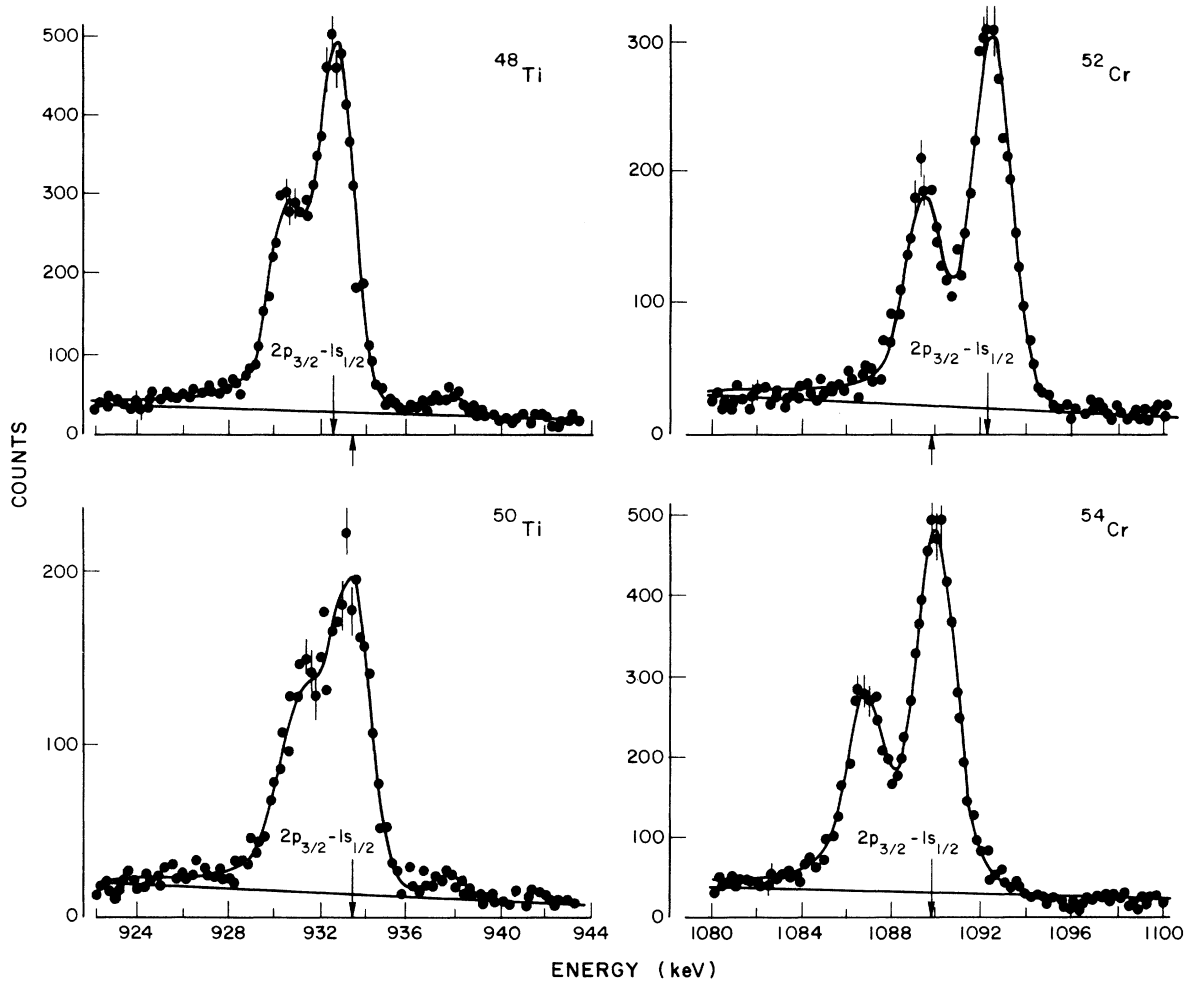

FIG. 2. Typical spectra showing the muonic $2p$-$1s$ x-ray doublet for Ti and Cr isotopes. The shifts of the x-ray energies are seen to have opposite signs for ^{50}Ti-^{48}Ti and ^{54}Cr-^{52}Cr. The substantial (24%) ^{48}Ti contamination of the ^{50}Ti target is visible. The curves show fits to the measured spectra. The weak line at about 937.5 keV is caused by feedthrough of the ^{110}Ag^{m} calibration source.

clude the uncertainty ($\leq$ 15 eV) of the nonlinearity correction.

In addition, best values for the $2p_{3/2}$-$1s_{1/2}$ absolute transition energies were determined as follows. In a second least squares adjustment, the transition energy of a single isotope was varied while the *transition energy differences* between the 21 nuclei were held fixed at the values from the first fit. This procedure yields a set of least squares adjusted *absolute transition energies* that are constrained to be consistent with the shift values. These transition energies are listed in Table IV. The χ^2 per degree of freedom of this adjustment was 1.05, a value which indicates that the influence of electronic instabilities and geometric effects on the measured transition energies and on their differences are small compared to the statistical error (25 eV) of a single measurement.

The uncertainties attached to the transition energies were obtained by quadratic addition of the following terms: (1) statistical error in the location of the line centroid; (2) a fitting error uncertainty ($\leq$ 15 eV) resulting from the fact that the fine-structure splitting was not resolved; (3) the uncertainty (5 eV) of the calibration energies; and (4) the uncertainty of the nonlinearity correction ($\leq$ 15 eV).

We note that the values given here for the $2p_{3/2}$-$1s_{1/2}$ transition energies of the Ca isotopes are 40 eV smaller than the values given in our previous publication.[12] This energy shift is due to including in the least squares energy adjustments the results of a high-precision remeasurement of ^{40}Ca performed after the publication of Ref. 12.

Table V compares the transition energies and

TABLE III. Least squares adjusted to $2p_{3/2}$-$1s_{1/2}$ energy differences (keV). The experimental uncertainty is listed under each value. Corrections have been applied for hyperfine splitting and isotopic impurities (see text). The values directly measured are in italics; all others are derived from the least squares adjustment.

					^{55}Mn	^{54}Cr	^{53}Cr	^{52}Cr	^{50}Cr	^{51}V	^{50}Ti	^{49}Ti	
^{41}K	*−0.349*												
	24												
^{40}Ca	*71.062*	71.411			*84.188*	*167.154*	165.661	164.756	*165.864*	244.841	323.454	323.616	^{56}Fe
	41	38			29	29	33	30	32	35	35	38	
^{42}Ca	70.251	70.600	*−0.811*			*82.966*	81.473	80.568	81.676	160.653	239.266	239.428	^{55}Mn
	43	40	16			28	32	29	33	34	32	35	
^{43}Ca	70.693	71.042	*−0.369*	*0.442*			*−1.493*	*−2.398*	−1.290	77.687	156.300	156.462	^{54}Cr
	42	39	15	16			22	20	27	30	31	35	
^{44}Ca	70.038	70.387	*−1.024*	*−0.213*	*−0.655*			*−0.905*	0.203	*79.180*	*157.793*	157.955	^{53}Cr
	41	38	13	16	14			19	28	26	30	34	
^{46}Ca	70.699	71.048	*−0.363*	0.448	0.006	0.661			*1.108*	*80.085*	*158.698*	*158.860*	^{52}Cr
	110	111	105	106	106	106			22	24	27	30	
^{48}Ca	71.369	71.718	*0.307*	*1.118*	0.676	*1.331*	0.670			78.977	157.590	157.752	^{50}Cr
	41	38	12	15	16	14	106			31	34	36	
^{45}Sc	143.877	144.226	72.815	73.626	73.184	*73.839*	73.178	72.508			*78.613*	*78.775*	^{51}V
	43	40	32	34	33	32	109	33			31	34	
^{46}Ti	218.876	219.225	*147.814*	148.625	148.183	*148.838*	148.177	147.507	*74.999*			0.162	^{50}Ti
	41	38	29	32	31	30	108	30	29			27	
^{47}Ti	219.356	219.705	*148.294*	149.105	148.663	149.318	148.657	147.987	*75.479*	*0.480*			
	41	38	29	32	31	30	108	31	29	19			
^{48}Ti	219.534	219.883	148.472	149.283	*148.841*	149.496	148.835	148.165	75.657	0.658	*0.178*		
	41	38	32	33	31	32	109	33	32	23	19		
^{49}Ti	220.308	220.657	149.246	150.057	149.615	150.270	149.609	148.939	76.431	1.432	*0.952*	*0.774*	
	46	43	36	38	37	37	110	37	36	29	25	27	
^{50}Ti	220.470	220.819	*149.408*	150.219	*149.777*	*150.432*	149.771	*149.101*	76.593	1.594	1.114	*0.936*	
	41	38	31	33	32	31	109	32	32	23	22	22	
^{51}V	299.083	299.432	228.021	228.832	228.390	229.045	228.384	227.714	155.206	80.207	79.727	79.549	
	41	38	36	38	36	36	110	36	35	35	34	35	
^{50}Cr	378.060	378.409	306.998	307.809	307.367	308.022	307.361	306.691	234.183	159.184	158.704	158.526	
	42	39	37	39	38	38	111	39	37	37	35	37	
^{52}Cr	379.168	379.517	308.106	308.917	308.475	309.130	308.469	307.799	235.291	160.292	159.812	159.634	
	38	35	33	35	33	33	110	33	32	32	30	31	
^{53}Cr	378.263	378.612	307.201	308.012	307.570	308.225	307.564	306.894	234.386	159.387	158.907	158.729	
	41	38	35	36	35	35	110	35	35	34	33	34	
^{54}Cr	376.770	377.119	305.708	306.519	306.077	306.732	306.071	305.401	232.893	157.894	157.414	157.236	
	45	42	35	37	36	35	111	36	35	35	33	35	
^{55}Mn	459.736	460.085	388.674	389.485	389.043	389.698	389.037	388.367	*315.859*	240.860	*240.380*	240.202	
	46	45	35	36	35	35	110	35	31	33	30	34	
^{56}Fe	543.924	544.273	472.862	473.673	473.231	473.886	473.225	472.555	400.047	325.048	324.568	324.390	
	41	38	35	38	37	36	110	36	36	36	35	36	
	^{39}K	^{41}K	^{40}Ca	^{42}Ca	^{43}Ca	^{44}Ca	^{46}Ca	^{48}Ca	^{45}Sc	^{46}Ti	^{47}Ti	^{48}Ti	

TABLE IV. Experimental equivalent radii R_k and Barrett moments $\langle r^k e^{-\alpha r}\rangle$ deduced from the $2p_{3/2}$-$1s_{1/2}$ transition energies. Fits were made using two-parameter Fermi charge distributions with a fixed at 0.55 fm. The theoretical nuclear polarization (NP) and quantum electrodynamic (QED) corrections used in the analysis are listed. The uncertainty in the nuclear polarization corrections, estimated to be 0.003 fm for the equivalent radii and 0.012 fm^k for the Barrett moments, are not included in the errors. The deduced rms radii are model dependent.

Isotope	Experimental transition energy (keV)	Correction NP (keV)	Correction QED (keV)	c (fm)	$\langle r^2\rangle^{1/2}$ (fm)	k	α (fm^{-1})	C_z (fm/keV)	R_k (fm)	C_z^* (fm^k/keV)	$\langle r^k e^{-\alpha r}\rangle$ (fm^k)
^{39}K	713.118(32)	0.145	5.324	3.5681	3.4378	2.114	0.064	−0.0499	4.4073(16)	−0.2276	10.666(7)
^{41}K	712.769(28)	0.150	5.305	3.5956	3.4549	2.114	0.064	−0.0499	4.4293(14)	−0.2276	10.767(6)
^{40}Ca	784.180(25)	0.170	5.907	3.6377	3.4813	2.114	0.065	−0.0420	4.4626(10)	−0.1922	10.879(5)
^{42}Ca	783.369(29)	0.196	5.891	3.6858	3.5115	2.114	0.065	−0.0420	4.5016(12)	−0.1922	11.057(6)
^{43}Ca	783.811(27)	0.181	5.897	3.6643	3.4980	2.114	0.065	−0.0420	4.4841(11)	−0.1922	10.977(5)
^{44}Ca	783.156(26)	0.205	5.886	3.7015	3.5214	2.114	0.065	−0.0420	4.5143(11)	−0.1922	11.116(5)
^{46}Ca	783.817(107)	0.208	5.897	3.6713	3.5024	2.114	0.065	−0.0420	4.4898(45)	−0.1922	11.003(21)
^{48}Ca	784.487(26)	0.190	5.905	3.6393	3.4823	2.114	0.065	−0.0420	4.4639(11)	−0.1922	10.884(5)
^{45}Sc	856.995(28)	0.233	6.489	3.7465	3.5498	2.116	0.066	−0.0356	4.5505(10)	−0.1649	11.270(5)
^{46}Ti	931.994(26)	0.285	7.093	3.8401	3.6094	2.118	0.068	−0.0307	4.6261(8)	−0.1419	11.563(4)
^{47}Ti	932.474(25)	0.265	7.099	3.8230	3.5984	2.118	0.068	−0.0307	4.6120(8)	−0.1419	11.498(4)
^{48}Ti	932.652(26)	0.284	7.103	3.8185	3.5956	2.118	0.068	−0.0307	4.6083(8)	−0.1419	11.481(4)
^{49}Ti	933.426(33)	0.237	7.113	3.7892	3.5770	2.118	0.068	−0.0307	4.5843(10)	−0.1419	11.370(5)
^{50}Ti	933.588(26)	0.253	7.114	3.7851	3.5743	2.118	0.068	−0.0307	4.5809(8)	−0.1419	11.354(4)
^{51}V	1012.201(26)	0.296	7.758	3.8307	3.6033	2.116	0.069	−0.0265	4.6173(7)	−0.1219	11.448(3)
^{50}Cr	1091.178(27)	0.392	8.391	3.9262	3.6645	2.115	0.071	−0.0232	4.6947(6)	−0.1063	11.698(3)
^{52}Cr	1092.286(21)	0.353	8.408	3.8962	3.6452	2.115	0.071	−0.0232	4.6698(5)	−0.1063	11.584(2)
^{53}Cr	1091.381(25)	0.342	8.391	3.9222	3.6620	2.115	0.071	−0.0232	4.6914(6)	−0.1063	11.683(3)
^{54}Cr	1089.888(31)	0.386	8.366	3.9661	3.6902	2.115	0.071	−0.0232	4.7278(7)	−0.1063	11.850(3)
^{55}Mn	1172.854(34)	0.396	9.041	3.9962	3.7096	2.120	0.072	−0.0203	4.7527(7)	−0.0945	11.999(3)
^{56}Fe	1257.042(25)	0.459	9.715	4.0449	3.7412	2.121	0.074	−0.0181	4.7921(5)	−0.0834	12.102(2)

TABLE V. Comparison with previous measurements. When necessary the values were converted from the $2p_{3/2}$-$1s_{1/2}$ transition energies to $2p$-$1s$ center of gravity values by subtracting $\frac{1}{3}$ of the theoretical fine-structure splitting. The $2p$-$1s$ center of gravity values for a natural target were calculated from the present values for separated isotopes taking into account the natural isotopic composition.

Isotope(s)	Measured quantity	Present value (keV)	Previous measurements (keV)	Ref.
^{nat}K	$2p$-$1s$ energy	712.690(32)	712.24 (40)	21
			712.64(23)	9
			712.654(20)	22
^{nat}Ca	$2p$-$1s$ energy	783.659(25)	784.00(40)	21
			783.85(15)	23
			783.56(16)	9
^{nat}Ti	$2p$-$1s$ energy	931.959(26)	931.57(40)	21
^{nat}V	$2p$-$1s$ energy	1011.342(26)	1011.3(2.3)	24
^{nat}Cr	$2p$-$1s$ energy	1091.081(27)	1094.4(4.3)	25
^{nat}Mn	$2p$-$1s$ energy	1171.666(35)	1171.2(4)	26
^{41}K-^{39}K	isotope shift	−0.349(24)	−0.350(60)	9
^{42}Ca-^{40}Ca	isotope shift	−0.811(16)	−0.690(60)	27
^{44}Ca-^{40}Ca	isotope shift	−1.024(13)	−0.890(50)	27
			−0.990(100)	20
^{48}Ca-^{40}Ca	isotope shift	0.307(12)	0.470(120)	27
^{52}Cr-^{50}Cr	isotope shift	1.108(22)	0.830(80)	20
^{53}Cr-^{52}Cr	isotope shift	−0.905(19)	−0.700(80)	20
^{54}Cr-^{52}Cr	isotope shift	−2.398(20)	−2.170(200)	20

isotope shifts determined from the present experiment with those from previous muonic x-ray measurements.[9,20-27] Our values for the $2p_{3/2}$-$1s_{1/2}$ transition energies, while in excellent agreement with previous measurements, are, in general, an order of magnitude more precise. In the case of the isotope shifts, the agreement is not always as good. The valus of Macagno *et al.*[20] for the ^{52}Cr-^{50}Cr and ^{53}Cr-^{52}Cr isotope shifts are substantially smaller than our values. Our result for the ^{44}Ca-^{40}Ca isotope shift is in good agreement with the result of Macagno *et al.*[20] but is, however, considerably larger than that of Ehrlich *et al.*[27]

III. NUCLEAR CHARGE RADII

A. Barrett moments and equivalent radii

Nuclear charge distribution parameters and their differences were derived from the measured $2p_{3/2}$-$1s_{1/2}$ transition energies and energy shifts using the methods described in Ref. 3. The half-density radius c of a two-parameter Fermi charge distribution

$$\rho_F(r) = \rho_0(1 + e^{(r-c)/a})^{-1} \tag{1}$$

was adjusted to reproduce the experimental transition energies; the skin-thickness parameter a was fixed at 0.55 fm.

The higher-order quantum electrodynamic and related corrections and the nuclear polarization corrections used in the analysis are listed in Table IV. These corrections were calculated with the computer programs MUON and RURP,[28] which use the methods of Refs. 29 and 30. The nuclear polarization corrections include the isoscalar and/or isovector contributions for multipoles $0 \leq L \leq 4$. The strength of each electric multipole was concentrated in a single resonance state whose energy was calculated by an empirical expression[28] and whose strength was determined by sum rules. The quadrupole contributions of the low lying 2^+ states have been included using the known energies and $B(E2)$ values of these states.[31] Owing to the use of different transition charge densities and other calculational differences, the nuclear polarization corrections used in this analysis are somewhat smaller than those used in Ref. 3 but agree with those of Ref. 3 within the uncertainty of 30% usually attributed to such calculations. The uncertainties of the quantum electrodynamic corrections are estimated[29] to be about 20 eV.

Table IV lists the fitted half-density radii c and the rms charge radii $\langle r^2\rangle^{1/2}$ derived from the two-parameter Fermi charge distribution. It should be emphasized that these rms radii, which have typical experimental errors of 0.0006 fm, are model dependent.

Model-independent Barrett moments $\langle r^k e^{-\alpha r}\rangle$ and equivalent radii R_k, defined by the equation

$$\langle r^k e^{-\alpha r}\rangle \equiv \frac{1}{Z}\int \rho_F(r) r^k e^{-\alpha r} 4\pi r^2 dr$$

$$= 3R_k^{-3}\int_0^{R_k} r^k e^{-\alpha r} r^2 dr\,, \tag{2}$$

were deduced from the adjusted Fermi charge distributions according to the method developed by Ford and Wills[32] and Barrett.[33] The parameters k and α are related to the difference in potential generated by the muon in the initial and final states of a particular muonic transition:

$$V^i(r) - V^f(r) = A + Br^k e^{-\alpha r}\,. \tag{3}$$

The values for k and α used in our analysis were taken from the compilation of Engfer *et al.*[34] to facilitate comparison with previous results. An adjustment of these parameters to correspond precisely to our measured transition energies resulted in values insignificantly different from those of Ref. 34. The errors of R_k and $\langle r^k e^{-\alpha r}\rangle$ are obtained by multiplying the experimental errors by the sensitivity factors $C_Z = dR_k/dE$ and $C_Z^* = d\langle r^k e^{-\alpha r}\rangle/dE$. The errors of the equivalent radii caused by uncertainties in the higher-order corrections to the muonic binding energies (chiefly the nuclear-polarization uncertainty) are estimated to be typically 0.003 fm; the corresponding errors of the Barrett moments are 0.012 fm^k. Table IV lists the values of k, α, C_Z, C_Z^*, and the model-independent equivalent radii and Barrett moments.

The isotope and isotone shifts ΔR_k listed in Table VI are the differences between the appropriate R_k values. The errors of ΔR_k were computed from the experimental errors of the energy differences (Table III) and the sensitivity factors C_Z. Because the higher-order corrections to the muonic binding energies vary slowly and smoothly with A and Z, the uncertainties of these corrections cancel to a large degree in the differences. Isotopic and isotonic variations of the higher-order corrections are mainly caused by contributions from low-lying $E2$ excitations to the nuclear polarization correction. The errors in ΔR_k caused by the uncertainties in the higher-order corrections are estimated[3] to be less than 0.001 fm.

B. Combined analysis of elastic electron-scattering and muonic data

To facilitate comparison of the muonic results with other experiments and with theory, model-independent rms charge radii $\langle r^2\rangle^{1/2}$ and their differences $\Delta\langle r^2\rangle^{1/2}$ were deduced from a combined analysis of the present muonic data and elastic

TABLE VI. Differences in equivalent radii R_k deduced from the $2p_{3/2}$-$1s_{1/2}$ isotope and isotone shifts. The calculated differences of rms radii are model-independent within the quoted errors. The uncertainty in the nuclear polarization corrections, estimated to be 0.001 fm for the radii differences, are not included in the errors.

Nuclei	ΔR_k (10^{-3} fm)	$\Delta\langle r^2\rangle^{1/2}$ (10^{-3} fm)	Nuclei	ΔR_k (10^{-3} fm)	$\Delta\langle r^2\rangle^{1/2}$ (10^{-3} fm)
^{41}K-^{39}K	22.0(1.2)	17.1(3.9)	^{43}Ca-^{42}Ca	−17.4(0.7)	−13.6(3.5)
^{42}Ca-^{40}Ca	38.9(0.7)	30.0(1.0)[a]	^{44}Ca-^{43}Ca	30.2(0.6)	23.4(3.5)
^{44}Ca-^{42}Ca	12.8(0.7)	11.4(1.6)[a]	^{47}Ti-^{46}Ti	−14.1(0.6)	−11.0(3.5)
^{46}Ca-^{44}Ca	−24.5(4.5)	−18.9(6.5)	^{48}Ti-^{47}Ti	−3.7(0.6)	−2.8(3.5)
^{48}Ca-^{46}Ca	−26.0(4.5)	−20.2(6.5)	^{49}Ti-^{48}Ti	−24.0(0.8)	−18.6(3.6)
^{48}Ti-^{46}Ti	−17.8(0.7)	−15.2(0.9)[a]	^{50}Ti-^{49}Ti	−3.4(0.8)	−2.7(3.6)
^{50}Ti-^{48}Ti	−27.4(0.7)	−22.8(1.2)[a]	^{53}Cr-^{52}Cr	21.6(0.4)	16.8(3.3)
^{52}Cr-^{50}Cr	−24.9(0.5)	−21.2(0.7)[a]	^{54}Cr-^{53}Cr	36.4(0.5)	28.2(3.4)
^{54}Cr-^{52}Cr	58.0(0.5)	46.6(0.7)[a]			
^{46}Ti-^{44}Ca	111.8(1.3)	89.6(2.1)[a]	^{40}Ca-^{39}K	55.3(2.0)	43.6(4.6)
^{48}Ti-^{46}Ca	118.5(4.6)	93.1(6.6)	^{42}Ca-^{41}K	72.3(2.0)	56.7(4.6)
^{50}Ti-^{48}Ca	117.0(1.3)	93.7(1.4)[a]	^{45}Sc-^{44}Ca	36.2(1.3)	28.4(4.0)
^{50}Cr-^{48}Ti	86.4(1.1)	68.9(3.9)	^{46}Ti-^{45}Sc	75.6(1.0)	59.6(3.8)
^{52}Cr-^{50}Ti	88.9(0.8)	70.9(3.6)	^{51}V-^{50}Ti	36.4(1.0)	29.0(3.7)
^{54}Fe-^{52}Cr[b]	66.9(0.9)	51.5(3.7)	^{52}Cr-^{51}V	52.5(0.6)	41.9(3.5)
^{56}Fe-^{54}Cr	64.3(0.7)	51.0(3.5)	^{55}Mn-^{54}Cr	24.9(0.6)	19.4(3.5)
			^{56}Fe-^{55}Mn	39.4(0.6)	31.6(3.5)

[a] Result of model-independent analysis (see text). All other rms-radii differences are deduced from Table IV with upper limit for model error (see text).

[b] Deduced from ^{56}Fe-^{52}Cr of this work and ^{56}Fe-^{54}Fe of Refs. 3 and 4.

electron-scattering data in those cases where the latter were available.

The method used in this combined analysis (described in detail in Ref. 4) is based on the Fourier-Bessel expansion[35] of the charge distribution:

$$\rho(r)=\begin{cases}\dfrac{Z}{4\pi}\displaystyle\sum_{\nu}a_\nu j_0(q_\nu r), & \text{for } r\le R_{\max}\\ 0, & \text{for } r>R_{\max}.\end{cases}\qquad(4)$$

In the framework of a plane-wave Born approximation, the parameters a_ν are related to the cutoff radius $R_{\max}$ and to the form factors $F(q_\nu)$ at momentum transfers $q_\nu=\pi\nu/R_{\max}$ by $a_\nu=2(\pi\nu)^2F(q_\nu)/R_{\max}^3$ [where the normalization of the charge distribution is $\int\rho(r)4\pi r^2dr=Z$]. For $\nu\le q_{\max}R_{\max}/\pi$, the a_ν are derived from the experimental data. Above $q_{\max}$, the a_ν are determined from an upper-bound estimate for the form factor.[35] In the present case, $\rho(r)$ was adjusted to simultaneously reproduce the elastic electron-scattering cross sections (via a phase-shift analysis) and the Barrett moment of the charge distribution. In effect, the combined analysis procedure provides a model-independent extrapolation from the precisely known and model-independent Barrett moment to yield a model-independent value for the $\langle r^2\rangle$ moment of the charge distribution.

In a similar way,[4] model-independent differences of charge distributions $\Delta\rho(r)$ and differences of rms radii $\Delta\langle r^2\rangle^{1/2}$ can be determined by exploiting the high accuracy of cross-section *ratios* and Barrett moment *differences*. In the present analysis, we used elastic electron-scattering cross-section ratios for ^{40}Ca/^{42}Ca, ^{40}Ca/^{44}Ca, ^{40}Ca/^{48}Ca, and ^{48}Ca/^{48}Ti from Frosch *et al.*,[8] for ^{46}Ti/^{48}Ti and ^{48}Ti/^{50}Ti from Heisenberg *et al.*,[36] and for ^{52}Cr/^{50}Cr and ^{54}Cr/^{52}Cr from Lightbody.[37] Additional cross-section ratios for other pairs of nuclei were generated as needed by taking appropriate products of the measured ratios.[38] A direct analysis of the Ti-Ca isotone differences was not possible, since the available electron-scattering data (Refs. 8 and 36) were obtained at different scattering energies. The charge distribution differences and rms radius differences of these pairs of nuclei were derived from analyses of other appropriate pairs [for example, $\Delta\rho(^{50}\text{Ti}\text{-}^{48}\text{Ca})=\Delta\rho(^{50}\text{Ti}\text{-}^{48}\text{Ti})-\Delta\rho(^{48}\text{Ca}\text{-}^{48}\text{Ti})$].

Table VI lists the model-independent rms charge radius differences derived from the combined analysis of the muonic and electron-scattering data and the $\Delta\langle r^2\rangle^{1/2}$ derived from Table IV for those nuclei for which no electron-scattering data were available. An upper limit for the error due to model dependency for these latter values was estimated by comparing the model-independent and model-dependent $\Delta\langle r^2\rangle^{1/2}$ values of those nuclei for which electron-scattering data were available. The largest difference so obtained (0.003 fm)

TABLE VII. Model-independent rms charge radii deduced from the combined analysis of the present muonic data and elastic electron scattering data of Refs. 8, 36, and 37. The major contribution to the error is due to the variation of $\langle r^2\rangle^{1/2}$ with cutoff radius. The error was estimated by varying R_{max} from 8 to 10 fm. The listed errors do not include the uncertainty in the nuclear polarization corrections, estimated to be 0.002 fm.

Nucleus	$\langle r^2\rangle^{1/2}$ (fm)
^{40}Ca	3.483(3)
^{42}Ca	3.513(3)
^{44}Ca	3.524(3)
^{48}Ca	3.482(3)
^{46}Ti	3.614(4)
^{48}Ti	3.599(4)
^{50}Ti	3.576(4)
^{50}Cr	3.666(3)
^{52}Cr	3.645(3)
^{54}Cr	3.691(3)

was adopted as a model error for the $\Delta\langle r^2\rangle^{1/2}$ derived from Table IV and was added linearly to the experimental error in those cases.

Table VII lists the model-independent rms charge radii deduced from the combined analysis of elastic electron-scattering and muonic data. The rms charge radii for ^{40}Ca and ^{52}Cr were determined from the absolute elastic electron-scattering cross sections and the absolute muonic $2p_{3/2}$-$1s_{1/2}$ transition energies. The radii for the other Ca isotopes and the Ti isotopes were determined from measured cross-section ratios and muonic $2p_{3/2}$-$1s_{1/2}$ isotope or isotone shifts relative to ^{40}Ca. The radii for ^{50}Cr and ^{54}Cr were determined relative to ^{52}Cr.

A comparison of the $\langle r^2\rangle^{1/2}$ and $\Delta\langle r^2\rangle^{1/2}$ deduced from the present experiment with the corresponding values from elastic electron-scattering data given in the compilation by De Jager *et al.*[39] shows that our values are in satisfactory agreement with the electron-scattering results and are more precise in all cases by at least a factor of 5.

IV. INTERPRETATION OF RESULTS

The primary aim of this investigation has been the systematic study of isotope and isotone shifts for the $1f_{7/2}$-shell nuclei. A summary of the results is shown in Figs. 3 and 4, which display the changes in rms charge radii produced by the addition of pairs of nucleons throughout the $1f_{7/2}$ proton and neutron shells. Plots of this type have been previously shown[40] to be quite useful in displaying the systematics of isotope shift data. In addition to the present results, data from Refs. 3 and 4 are included in Figs. 3 and 4 to portray the systematic behavior of all $1f_{7/2}$-shell nuclei.

A. Charge radii

1. Observed systematics

The sequential addition of proton pairs to the $1f_{7/2}$ orbital, shown in Fig. 3, results in an almost linear decrease in the successive isotone shifts. Furthermore, it is apparent that the isotone shifts are independent of the neutron configuration of the nuclei involved. For example, the ^{46}Ti-^{44}Ca, ^{48}Ti-^{46}Ca, and ^{50}Ti-^{48}Ca isotone shifts are all identical within the experimental uncertainties. We find this behavior quite remarkable, particularly in view of the high precision of the data.

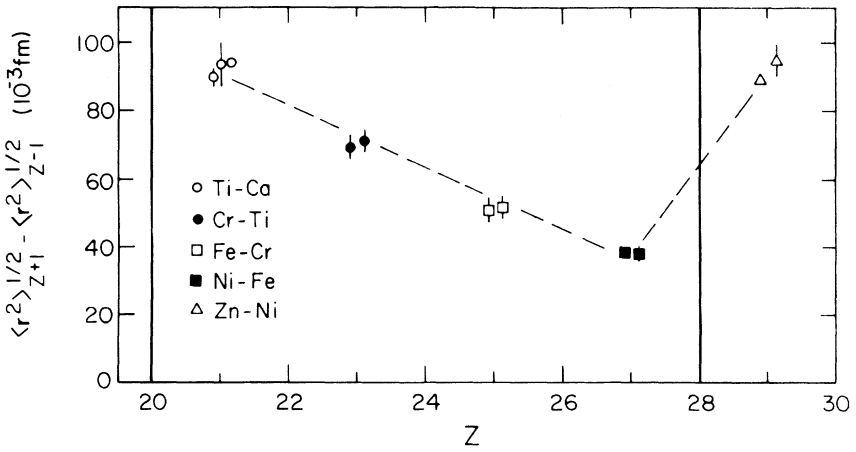

FIG. 3. Model-independent isotonic $\Delta Z=2$ rms charge radii differences. The values and their errors have been deduced from a combined analysis of elastic electron-scattering data with present (see Table VI) and previous (see Refs. 3 and 4) muonic x-ray data.

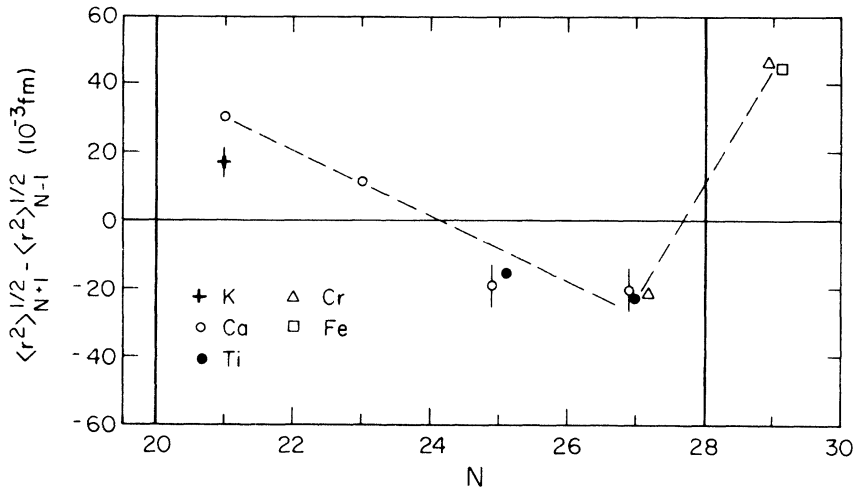

FIG. 4. Model-independent isotopic $\Delta N = 2$ rms charge radii differences. See the caption of Fig. 3.

A sudden increase in the isotone shifts, more than a factor of 2, occurs at $Z = 28$, while neutron-configuration independence is maintained. Such abrupt changes in the magnitude of the isotone and isotope shifts have been previously shown[3] to be associated with the shell structure of nuclei. In the present case, the sudden increase reflects the beginning of the $2p_{3/2}$ shell.

The $1f_{7/2}$-shell isotope shifts, shown in Fig. 4, display many of the features of the $1f_{7/2}$-shell isotone shifts. The sequential addition of neutron pairs to the $1f_{7/2}$ orbital causes an increase in the rms radii in the first half of the $1f_{7/2}$ neutron shell and a decrease in the second half. The net result is a linear decrease in the successive isotope shifts, which (for the even-A isotope pairs) are independent of the proton configuration. This feature of the isotope shifts is even more remarkable than the similar behavior of the isotone shifts since, in the isotope-shift case, different proton cores are involved. An abrupt increase in the isotope shifts, like that in the isotone shifts at $Z = 28$, occurs at $N = 28$, reflecting the beginning of the $2p_{3/2}$ neutron shell. The $\Delta N = 2$ isotope shift of the odd-Z nuclei ^{41}K-^{39}K departs somewhat from the corresponding even-even isotope shift. This presumably results from the odd-even staggering effect.

The odd-even staggering behavior of the $1f_{7/2}$ nuclei can be seen in Table VIII in which the measured $\Delta A = 1$ shifts are listed in terms of the odd-even staggering parameter

$$\gamma_{A+1} = 2\frac{\langle r^2\rangle_{A+1} - \langle r^2\rangle_A}{\langle r^2\rangle_{A+2} - \langle r^2\rangle_A}. \quad (5)$$

The staggering effect is manifest as a deviation of γ from unity, the value expected if the addition of one nucleon resulted in one-half the shift due to the addition of a pair of nucleons. All the listed γ values exhibit a significant odd-even staggering effect; this topic will be considered further in Sec. IV A 4.

2. *Comparison of isotone and isotope shifts – core polarization*

The data summarized in the preceding section provides, for the first time, an opportunity to study the behavior of isotone shifts over a wide range of nuclei. Isotone shifts, in contrast to isotope shifts, are dominated by the charge of the added protons. Thus, before isotope- and isotone-shift data can be compared on an equivalent basis, the charge distribution of the added protons must first be considered. Elastic electron-scattering experiments[4] have shown that the radial dependence of $\Delta\rho(r)$ between $1f_{7/2}$-shell isotones is well-de-

TABLE VIII. Measured odd-even staggering parameters [see Eq. (5)]. The listed uncertainties include possible model errors (see Table VI). The experimental errors are smaller by about a factor of 5.

Sequence of nuclei	γ_{A+1}
Isotopes	
^{42}Ca-^{43}Ca-^{44}Ca	−2.39(70)
^{46}Ti-^{47}Ti-^{48}Ti	1.46(47)
^{48}Ti-^{49}Ti-^{50}Ti	1.63(33)
^{52}Cr-^{53}Cr-^{54}Cr	0.75(16)
Isotones	
^{44}Ca-^{45}Sc-^{46}Ti	0.63(9)
^{50}Ti-^{51}V-^{52}Cr	0.82(11)
^{54}Cr-^{55}Mn-^{56}Fe	0.76(14)

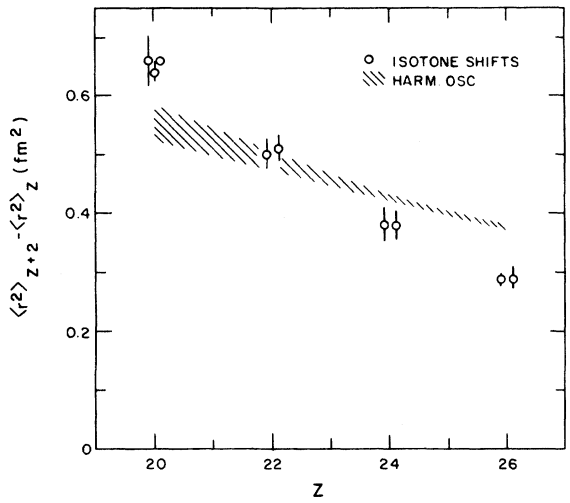

FIG. 5. Experimental isotone shifts compared with a harmonic oscillator shell model calculation. Core polarization is neglected. Because the isotone shifts are essentially independent of N, we have grouped certain isotone pairs together, in analogy with Fig. 3.

scribed by $1f_{7/2}$-shell harmonic oscillator wave functions. As a zeroth-order approximation, we therefore calculated a set of $1f_{7/2}$-shell isotone shifts considering only the charge distribution of the added protons. The $1f_{7/2}$-shell protons were represented by harmonic oscillator wave functions [the potential parameter $b^2 = 41.44/(45A^{-1/3} - 25A^{-2/3})$ fm^2 was taken from Blomqvist and Molinari[41]] The results are compared with the measured isotone shifts in Fig. 5. It is evident that the zeroth-order calculation is in qualitative agreement with experiment. As expected, it correctly predicts a "saturation" of the isotone shifts as (identical) protons are added to the $1f_{7/2}$ shell. We observe, however, that the actual isotone shifts decrease more rapidly with increasing Z than the harmonic oscillator calculation would suggest.

It is evident that the effect of the added nucleons on the proton core must be included when considering either isotone or isotope shifts. In the case of isotope shifts, this "core polarization" is, in fact, the dominant effect. Allowing for core polarization, we can relate the charge distribution densities of two nuclei which differ by two protons by

$$\rho_{Z+2} = \rho_Z + 2\rho_p + \Delta\rho_Z^{\text{core}} \quad , \tag{6}$$

where ρ_p is the spatial distribution of the added protons and $\Delta\rho_Z^{\text{core}}$ describes the polarization of the ρ_Z core by the added protons.

An expression for the change in $\langle r^2\rangle$ caused by the interaction of the core with the added protons, $\Delta\langle r^2\rangle_Z^{\text{core}}$, can be derived from Eq. (6):

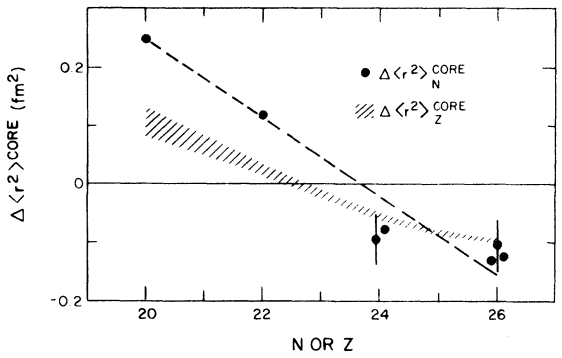

FIG. 6. Comparison of the neutron-produced core polarization (corrected for the neutron form factor and the spin-orbit effect) with the proton-produced core polarization calculated with Eq. (7).

$$\Delta\langle r^2\rangle_Z^{\text{core}} = \frac{Z+2}{Z}(\langle r^2\rangle_{Z+2} - \langle r^2\rangle_Z) + \frac{2}{Z}(\langle r^2\rangle_Z - \langle r^2\rangle_p - \langle r_p^2\rangle) . \tag{7}$$

Here $\langle r^2\rangle_p$ is the point proton mean-square radius of the valence protons and $\langle r_p^2\rangle$ is the mean-square radius of the proton. For each of the $1f_{7/2}$-shell isotone pairs we have obtained the value of $\Delta\langle r^2\rangle^{\text{core}}$ from the experimentally determined isotone shift $\langle r^2\rangle_{Z+2} - \langle r^2\rangle_Z$ and mean-square radius $\langle r^2\rangle_Z$, using the value[42] of 0.70 fm^2 for $\langle r_p^2\rangle$ and using the harmonic oscillator wave function discussed above to compute $\langle r^2\rangle_p$. The results are shown in Fig. 6. The proton-produced core polarization is positive in the first half of the shell and negative in the second half. It has the same trend as the core polarization caused by added neutrons $\Delta\langle r^2\rangle_N^{\text{core}}$, which is shown for the even nuclei by the points in Fig. 6. The core polarization caused by the added neutrons was obtained by correcting the measured isotope shifts for the neutron charge form factor and the spin-orbit interaction with the formula given by Bertozzi *et al.*[43] The proton-produced core polarization is on the average about 50% smaller than the neutron-produced core polarization. We conclude that, when the charge distributions of the added nucleons themselves are appropriately considered, isotope- and isotone-shift data can be usefully compared and that the two types of measurements reveal qualitatively similar polarization behavior in the $1f_{7/2}$ shell.

3. *Phenomenological charge radius formulas*

Zamick[44] has proposed a formula for the mean-square charge radii of singly closed-shell nuclei

in analogy with a formula obtained by Talmi and Unna[45] for binding energies. In the case of the $1f_{7/2}$ shell, the Zamick formula is

$$\Delta\langle r^2\rangle_{20+n} = \langle r^2\rangle_{20+n} - \langle r^2\rangle_{20}$$
$$= nC + \frac{n(n-1)}{2}\alpha + \left[\frac{n}{2}\right]\beta , \qquad (8)$$

where

$$\left[\frac{n}{2}\right] = \begin{cases} n/2, & \text{for even } n \\ (n-1)/2, & \text{for odd } n . \end{cases}$$

It describes the change of the mean-square charge radius $\Delta\langle r^2\rangle$ caused by addition of n particles to the shell. This formula considers, in Zamick's terminology, one-body (parameter C) and two-body (parameters α and β) interactions of the added particles with the core. The formula is represented by two parabolas, one for even-n and one for odd-n nuclei. The parabolas are shifted by $\beta/2$ because of the pairing effect. As proposed, the formula applies to the mean-square radius of a nucleus with only protons (or only neutrons) outside closed shells.

We have extended Zamick's formula to all $1f_{7/2}$ nuclei, including those with both neutrons and protons outside closed shells. This procedure is justified by our experimental results, which show that the isotope (isotone) shifts are independent of the proton (neutron) configuration. The parameters C, α, and β of Eq. (8) were adjusted separately to the experimental isotope and isotone shifts. The $\Delta\langle r^2\rangle$ and their errors were calculated from the data of Tables IV, VI, and VII. In the isotope-shift fit, the ^{41}K-^{39}K isotope shift was excluded; in the isotone-shift fit, the results of Refs. 3 and 4 for the nuclei ^{54,56,58}Fe, ^{59}Co, and ^{58,60}Ni were included. The parameter values that best fit the experimental isotope and isotone shifts are listed in Table IX. The parameters α and β are the same for protons and neutrons within their errors. The difference in the parameter C for protons and neutrons reflects the fact that the isotone shifts include both the spatial distribution of the valence protons and polarization of the core, whereas the isotope shifts include only the latter effect.

TABLE IX. Adjusted parameters of Eq. (8).

	C (10^{-2} fm^2)	α (10^{-2} fm^2)	β (10^{-1} fm^2)
Isotopes	1.9(1.5)	−3.20(5)	1.87(30)
Isotones	25.5(1.3)	−3.10(11)	1.67(27)

In Fig. 7 the experimental results for the isotope and isotone shifts are compared with values computed from Eq. (8) using the fitted values of C, α, and β. For the isotone shifts, the effect of the spatial distribution of the valence protons $\langle r^2\rangle_p^{\text{eff}}$ has been subtracted. The magnitude of this effect, 0.231 fm^2/proton, was deduced as an average over the $1f_{7/2}$ shell from a shell-model calculation using $1f_{7/2}$ harmonic oscillator wave functions. By so allowing for $\langle r^2\rangle_p^{\text{eff}}$, we obtain from Eq. (8) a value of C_{isotone} [0.024 ± 0.013 fm^2] that is quite similar to that of C_{isotope} [0.019 ± 0.015 fm^2]. The agreement shown in Fig. 7, while not as impressive as that obtained by Talmi and Unna[45] for the binding energies, shows that Eq. (8) describes the observed systematics surprisingly well. We can predict from Eq. (8) that $\Delta\langle r^2\rangle = 0.019 \pm 0.015$ fm^2 for ^{41}Ca-^{40}Ca and $\Delta\langle r^2\rangle = 0.149 \pm 0.016$ fm^2 for ^{45}Ca-^{40}Ca. These predictions agree quite satisfactorily with values obtained from a recent optical isotope-shift measurement by Bergmann *et al.*,[46] who obtained values for these isotope shifts of 0.003 ± 0.003 fm^2 and 0.127 ± 0.010 fm^2, respectively.

Combining the separate adjustments to the isotope and isotone shifts and using the ^{40}Ca rms radius from Table VII, one can obtain a general empirical formula for the rms charge radii of the

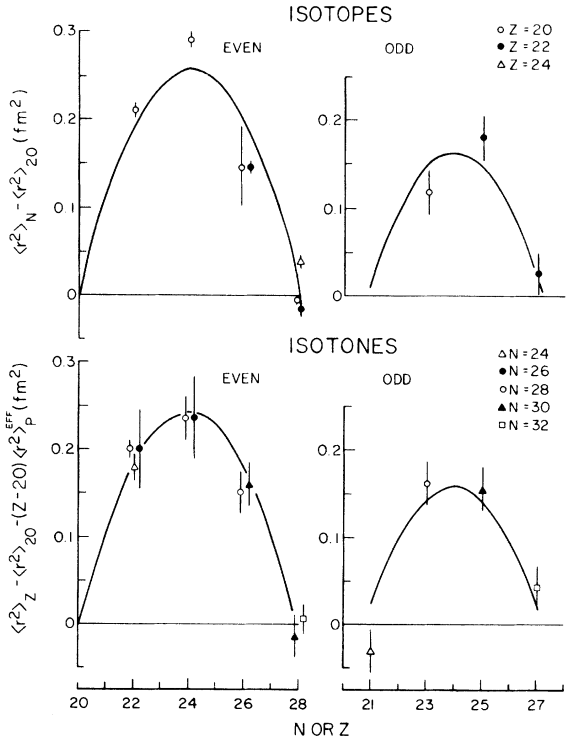

FIG. 7. Comparison of isotope- and isotone-shift data with predictions of Eq. (8) (see text).

$1f_{7/2}$-shell nuclei:

$$\langle r^2\rangle_{N,Z}^{1/2} = (\langle r^2\rangle_{20,20} + \Delta\langle r^2\rangle_{20+n} + \Delta\langle r^2\rangle_{20+z})^{1/2}$$
$$= \Big(12.1313 + 0.0192n - 0.0160n(n-1) + 0.1866\left[\frac{n}{2}\right] + 0.2550z - 0.0155z(z-1) + 0.1673\left[\frac{z}{2}\right]\Big)^{1/2} \text{ fm}, \quad (9)$$

where $n = N - 20$ and $z = Z - 20$. This formula reproduces the experimental $\langle r^2\rangle^{1/2}$ values of all measured $1f_{7/2}$-shell nuclei ($20 \le N \le 28$, $20 \le Z \le 28$) with an average error of less than 0.003 fm.

4. *Deformation effects*

Generally, changes in isotope and isotone shifts have been interpreted as resulting from two effects: (1) a change in volume of the charge distribution and (2) a change in deformation of the nucleus. The deformation effect was first suggested by Brix and Kopfermann[47] to account for anomalously large isotope shifts observed between rare-earth isotopes in early optical isotope-shift experiments. The incompressible fluid model of the nucleus has been used to correlate $\Delta\langle r^2\rangle$ with these two effects (see, for example, Ref. 48). To investigate the relationship between our measured isotope and isotone shifts and nuclear deformation, we have computed values of the quadrupole deformation parameter β^2 for the even $1f_{7/2}$-shell nuclei. In the computations we assumed the usual vibrational-model relationship between β^2 and the experimental ground-to-2^+ state $B(E2)$ value. The resulting deformation differences for isotopes and isotones are plotted in Fig. 8.

The similarity between Fig. 8 and the isotope and isotone shift plots (Figs. 3 and 4) is immediately apparent. *All* the features that were discussed in connection with the isotope- and isotone-shift systematics also appear, albeit with poorer experimental precision, in Fig. 8. The magnitude of the $\Delta\beta^2$ values, like the core polarization effect shown in Fig. 6, is approximately twice as large for isotopes as for isotones. Thus, the correlation between $\Delta\langle r^2\rangle$ and $\Delta\beta^2$ implied by the simple incompressible fluid model appears to be supported, at least qualitatively for the $1f_{7/2}$-shell nuclei, by experimental evidence. This observation has been given a microscopic basis through a recent calculation by Reinhard and Drechsel,[49] which is discussed in Sec. IV C.

The importance of deformation effects is reflected, in a more subtle way, in the ^{41}K-^{39}K isotope shift and the observed odd-even staggering parameters. Reehal and Sorensen[50] have suggested that the odd-even staggering effect occurs because the deformation associated with the zero-point quadrupole oscillations is smaller for odd nuclei than for even nuclei due to the blocking effect of the unpaired nucleon. One might therefore expect the odd-even staggering parameters to be smaller than unity in the first half of the $1f_{7/2}$ shell (where the deformation is increasing) and larger than unity in the second half (where the deformation is decreasing). The observed odd-even staggering effects in the isotope shifts are in qualitative agreement with this expectation (see Table VIII). At first glance, the odd-even staggering effects in the isotone shifts seem to disagree. In this case, however, the blocking effect is hidden by the spatial distribution of the protons. When the effect of the valence protons is subtracted, one indeed obtains odd-even staggering parameters for the isotone shifts in agreement with our expectation. Similarly, the ^{41}K-^{39}K isotope shift is expected (and found) to be smaller than that of ^{42}Ca-^{40}Ca because the contribution to $\Delta\langle r^2\rangle^{1/2}$ caused by deformation changes in the even Ca nuclei should be partially blocked by the proton hole in the K nuclei.

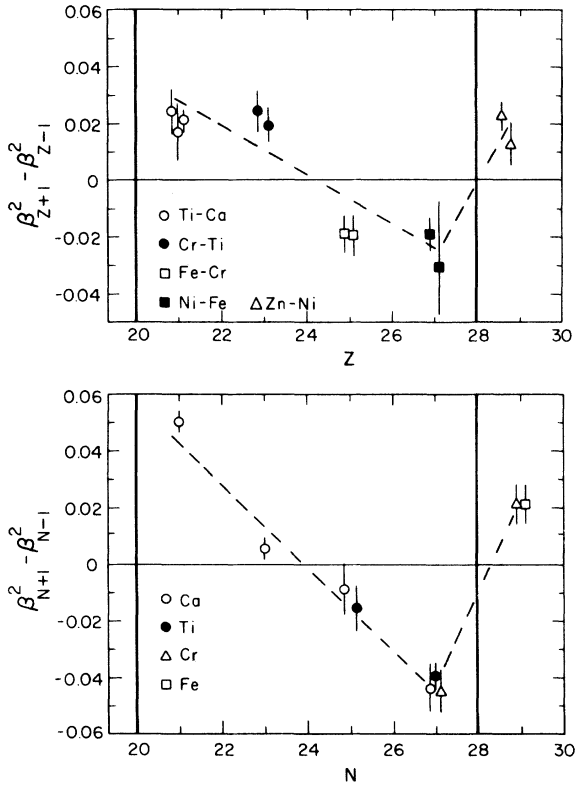

FIG. 8. Quadrupole deformation changes between $\Delta Z = 2$ and $\Delta N = 2$ pairs of even $1f_{7/2}$-shell nuclei as functions of Z and N, respectively. Values of β^2 have been calculated from measured $B(E2)$ values (Ref. 31). The similarity with Figs. 3 and 4 is apparent.

B. Model-independent charge distribution differences

Figure 9 shows certain charge distribution differences deduced from the combined model-independent analysis of the muonic and elastic electron-scattering data. The method used to derive the $r^2\Delta\rho(r)$ is described in Sec. III B. The charge distribution difference of ^{44}Ca-^{40}Ca shows the polarization of the $Z=20$ proton core produced by the first four neutrons added to the $1f_{7/2}$ shell. As can be seen, charge from the inner part of the nucleus is moved to the outer part, with a resulting increase in the rms charge radius. The charge distribution differences of ^{48}Ca-^{44}Ca and ^{50}Ti-^{46}Ti show the interaction of the last four neutrons added to the $1f_{7/2}$ shell with $Z=20$ and $Z=22$ proton cores, respectively. In both cases, charge from the outer part of the nucleus moves to the inner part, causing a decrease in the rms charge radius. Taking into account the normalization $\int\rho(r)4\pi r^2dr = Z$, the charge distribution differences of ^{48}Ca-^{44}Ca and ^{50}Ti-^{46}Ti are almost identical, indicating that $\Delta\langle r^2\rangle^{1/2}$ is independent of the proton configuration and suggesting that the added neutrons interact with the whole proton core, rather than with the valence protons. Similar behavior has been observed in $2p_{3/2}$- and $1f_{5/2}$-shell isotopes.[3,4]

The charge distribution difference for ^{48}Ca-^{40}Ca, shown in Fig. 9, represents the sum of the two effects discussed above. By adding eight neutrons to ^{40}Ca, charge from both the inner and the outer part of the proton core is transferred to the surface region. A fortuitous cancellation is apparently responsible for the well-known fact that the rms charge radii of ^{40}Ca and ^{48}Ca are essentially identical.

C. Comparison with calculations

The doubly closed-shell nuclei ^{40}Ca and ^{48}Ca have been the subjects of many theoretical calculations. The results of several such calculations of the rms charge radius difference of ^{48}Ca-^{40}Ca were compared with our experimental value in Ref. 12. Some recent Hartree-Fock (HF) calculations[51,52] are in better agreement with experiment than those presented in that reference. As an example, a density-dependent Hartree-Fock (DDHF) calculation of Negele[51] compares satisfactorily with the experimental charge distribution difference of ^{48}Ca-^{40}Ca as shown in Fig. 10. Although the absolute charge radii of ^{40}Ca and ^{48}Ca given by this calculation are slightly too large, the ^{48}Ca-^{40}Ca charge radius difference of −0.003 fm is in satisfactory agreement with the experimental value (−0.0007 ± 0.0009 fm). The mean-field approximation used in HF calculations is not strictly applicable even to ^{40}Ca since the calculations of Refs. 53 and 54 have indicated that

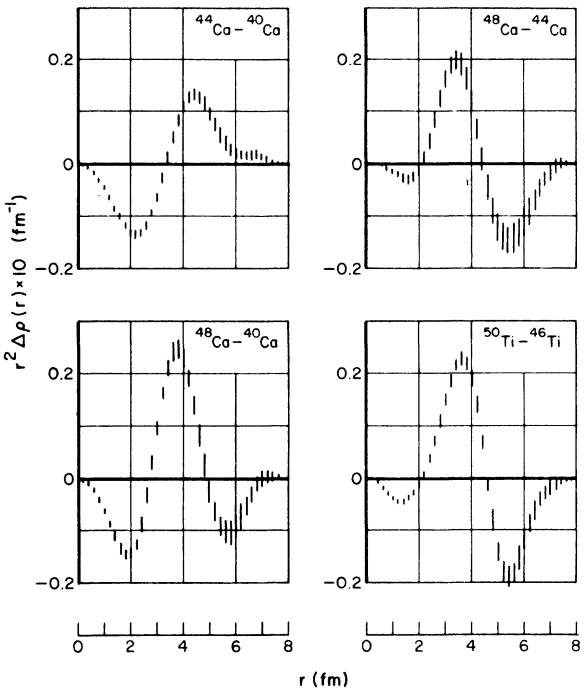

FIG. 9. Charge distribution differences for certain $1f_{7/2}$-shell nuclei from a combined model-independent analysis of the present muonic data and the elastic electron-scattering data of Refs. 8 and 36. The error bars include both experimental and incompleteness errors.

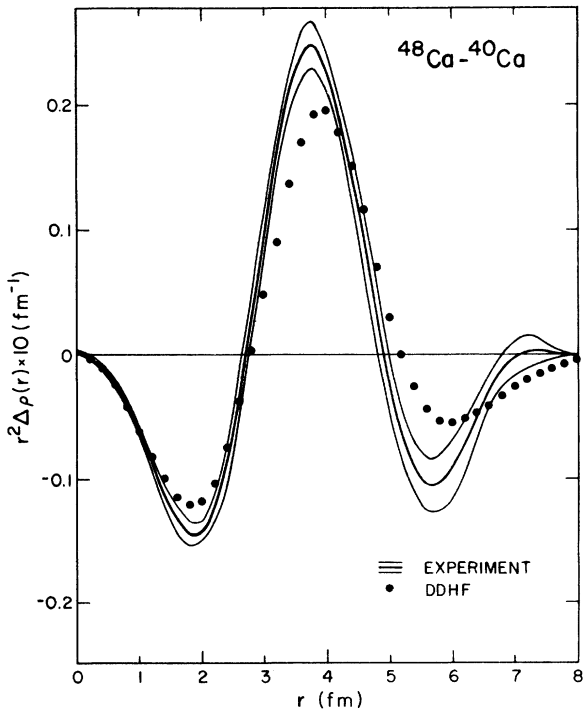

FIG. 10. DDHF calculation of the ^{48}Ca-^{40}Ca charge distribution difference (Ref. 51) compared with experiment.

^{40}Ca has a poorly closed *sd* shell. Recent DDHF calculations by Dechargé and Gogny for ^{40}Ca (see Ref. 55), in which random-phase-approximation correlations are included, show that particle-hole excitations have a considerable effect. These calculations indicate a depopulation of the 2*s* shell in favor of the 1*f* shell, which reduces the oscillatory component of $\rho(r)$ at small radii obtained from other DDHF calculations. The reduced oscillation at small radii is in better agreement with the experimental $\rho(r)$ deduced from an analysis of muonic data and recent high-momentum-transfer electron-scattering data from Saclay.[56]

For the isotope shifts of Ca, other than that of ^{48}Ca-^{40}Ca, the conventional HF approach agrees rather poorly with the measured $\Delta\rho(r)$ and $\Delta\langle r^2\rangle^{1/2}$ values. Brown *et al.*[57] have suggested that a probable fault in these calculations is that non-closed-shell configurations are ignored. By using the muonic $\Delta\langle r^2\rangle^{1/2}$ to adjust the amount of excitation from the *sd* shell to the *fp* shell for the different Ca isotopes, they obtain improved agreement between the experimental and calculated $\Delta\rho(r)$.

Reinhard and Drechsel[49] have recently calculated $\Delta\langle r^2\rangle^{1/2}$ for the Ca isotopes. Combining a sum rule approach and the generator-coordinate method, they consider the influence of ground-state correlations on the radial charge distribution. Their calculation results in a simple expression for the isotope shifts, which involve spherical HF calculations and the experimental $B(E2)$ values to the lowest 2^+ states. Figure 11 shows the results of their calculations.[58] The HF term makes a smoothly varying and almost constant contribution to $\Delta\langle r^2\rangle^{1/2}$. The $B(E2)$-related term, which is identical to the corresponding term in the usual incompressible fluid model formulation,[48] introduces a strong variation in the predictions for different Ca isotopes. As suggested by the similarity of Figs. 4 and 8, this term substantially improves the agreement between theory and experiment.

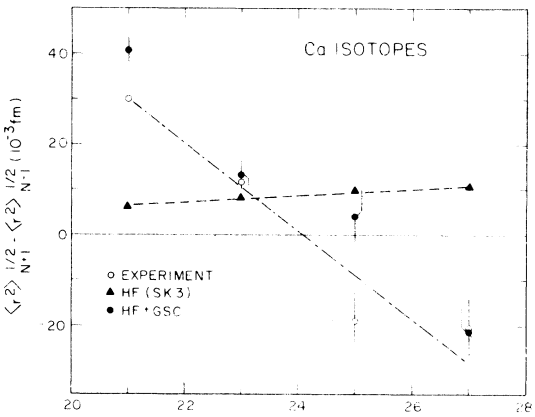

FIG. 11. Calculated isotope shifts for Ca (Ref. 49) compared with experiment. The triangles show the results of a pure HF calculation using the Skyrme 3 force. The solid circles include the effect of ground-state correlations calculated from experimental $B(E2)$ values.

This work was supported by the U. S. Department of Energy.

*Present affiliation: National Laboratory for High Energy Physics (KEK), Oho-Machi, Tsukuba-un, Ibaraki-Ken 300-32, Japan.

[1]H. R. Collard, L. R. B. Elton, and R. Hofstadter, *Nuclear Radii in Landolt-Börnstein, Numerical Data and Functional Relationships in Science and Technology*, edited by K.-H. Hellwege (Springer, Berlin, 1967), New Series, Group I, Vol. 2.

[2]W. D. Myers, Nucl. Phys. A204, 465 (1973).

[3]E. B. Shera, E. T. Ritter, R. B. Perkins, G. A. Rinker, L. K. Wagner, H. D. Wohlfahrt, G. Fricke, and R. M. Steffen, Phys. Rev. C 14, 731 (1976).

[4]H. D. Wohlfahrt, Habilitationsschrift, University of Mainz, 1976 (unpublished); H. D. Wohlfahrt, O. Schwentker, G. Fricke, H. G. Andresen, and E. B. Shera, Phys. Rev. C 22, 264 (1980).

[5]I. Angeli and M. Csatlos, Nucl. Phys. A288, 480 (1977).

[6]I. Angeli and M. Csatlos, ATOMKI Kozl. 20, 1 (1978).

[7]J. W. Negele and G. Rinker, Phys. Rev. C 15, 1499 (1977).

[8]R. F. Frosch, R. Hofstadter, J. S. McCarthy, G. K. Noldecke, K. J. Van Oostrum, M. R. Yearian, B. C. Clark, R. Herman, and D. G. Ravenhall, Phys. Rev. 174, 1380 (1968).

[9]R. D. Ehrlich, Phys. Rev. 173, 1088 (1968).

[10]R. Neumann, F. Träger, J. Kowalski, and G. zu Putlitz, Z. Phys. A 279, 249 (1976).

[11]H. W. Brandt, K. Heilig, H. Knöckel, and A. Steudel, Phys. Lett. A64, 29 (1977).

[12]H. D. Wohlfahrt, E. B. Shera, M. V. Hoehn, Y. Yamazaki, G. Fricke, and R. M. Steffen, Phys. Lett. B 73, 131 (1978).

[13]J. W. Negele, Phys. Rev. C 1, 1260 (1970).

[14]L. D. Miller and A. E. S. Green, Phys. Rev. C 5, 241 (1973).

[15]D. Vautherin and D. M. Brink, Phys. Rev. C 5, 626 (1972).

[16]J. W. Ehlers and S. A. Moszkowski, Phys. Rev. C 6, 217 (1972).

[17]Y. Yamazaki, E. B. Shera, M. V. Hoehn, and R. M. Steffen, Phys. Rev. C 18, 1474 (1978).

[18]R. G. Helmer, R. C. Greenwood and R. J. Gehrke, Nucl. Instrum. Methods 155, 189 (1978); R. C. Greenwood, R. G. Helmer, and R. J. Gehrke, *ibid.* 159, 465 (1979).

[19]G. H. Fuller and V. W. Cohen, Nucl. Data, Sect. A 5,

433 (1969); G. H. Fuller, J. Phys. Chem. Ref. Data 5, 838 (1976).
[20]E. R. Macagno, S. Bernow, S. C. Cheng, S. Devons, I. Duerdoth, D. Hitlin, J. W. Kast, W. Y. Lee, J. Rainwater, C. S. Wu, and R. C. Barrett, Phys. Rev. C 1, 1202 (1970).
[21]T. T. Bardin, R. C. Barrett, R. C. Cohen, S. Devons, D. Hitlin, E. R. Macagno, C. Nissim-Sabat, J. Rainwater, K. Runge, and C. S. Wu, Columbia Report Nos. GEN-72, ONR 266 (72), 1966 (unpublished).
[22]L. A. Schaller, T. Dubler, K. Kaeser, G. A. Rinker, Jr., B. Robert-Tissot, L. Schellenberg, and H. Schneuwly, Nucl. Phys. A300, 225 (1978).
[23]A. Suzuki, Phys. Rev. Lett. 19, 1005 (1967).
[24]J. A. Bjorkland, S. Raboy, C. C. Trail, R. D. Ehrlich, and R. J. Powers, Nucl. Phys. 69, 161 (1965).
[25]C. S. Johnson, E. P. Hincks, and H. L. Anderson, Phys. Rev. 125, 2102 (1962).
[26]D. Quitmann, R. Engfer, U. Hegel, P. Brix, G. Backenstoss, K. Goebel, and B. Stadler, Nucl. Phys. 51, 609 (1964).
[27]R. D. Ehrlich, D. Fryberger, D. A. Jensen, C. Nissim-Sabat, R. J. Powers, V. L. Telegdi, and C. K. Hargrove, Phys. Rev. Lett. 18, 959 (1967).
[28]G. A. Rinker, Comput. Phys. Commun. 16, 221 (1978).
[29]G. A. Rinker and R. M. Steffen, At. Data Nucl. Data Tables 20, 143 (1977).
[30]G. A. Rinker and J. Speth, Nucl. Phys. A306, 397 (1978).
[31]P. H. Stelson and L. Grodzins, Nucl. Data, Sect. A 1, 21 (1965); A. Christy and O. Hansen, Nucl. Data Tables 11, 281 (1972).
[32]K. W. Ford and J. G. Wills, Phys. Rev. 185, 1429 (1969).
[33]R. C. Barrett, Phys. Lett. B33, 388 (1970).
[34]R. Engfer, H. Schneuwly, J. L. Veuilleumier, H. K. Walter, and A. Zehnder, At. Data Nucl. Data Tables 14, 509 (1974).
[35]B. Dreher, J. Friedrich, K. Merle, H. Rothhaas, and G. Lührs, Nucl. Phys. A235, 219 (1974).
[36]J. Heisenberg, R. Hofstadter, J. S. McCarthy, R. Herman, B. C. Clark, and D. G. Ravenhall, Phys. Rev. C 6, 381 (1972).
[37]J. W. Lightbody, National Bureau of Standards, 1979 (private communication).
[38]In the combined analysis the differences of the Barrett moments were used to determine the relative normalization of the elastic electron-scattering cross-section ratios. This led to a significantly improved adjustment of the cross-section ratios and removed small unphysical structures in the $\Delta\rho(r)$ obtained with the original electron data. The small changes in the $\Delta\langle r^2\rangle^{1/2}$ of the Ca isotopes from the values given in Ref. 12 are due to this new analysis.
[39]C. W. DeJager, H. DeVries, and C. DeVries, At. Data Nucl. Data Tables 14, 479 (1974).
[40]P. Brix and H. Kopfermann, Festschrift Akad. Wiss. Gottingen, Math.-Phys. Kl., 17 (1951).
[41]J. Blomqvist and A. Molinari, Nucl. Phys. A106, 545 (1968).
[42]G. Höhler, E. Pietarinen, I. Sabbri-Slefanescu, F. Borkowsky, G. G. Simon, V. H. Walther, and R. Wendling, Nucl. Phys. B114, 505 (1976).
[43]W. Bertozzi, J. Friar, J. Heisenberg, and J. W. Negele, Phys. Lett. B41, 408 (1972).
[44]L. Zamick, Ann. Phys. (N.Y.) 66, 784 (1971).
[45]I. Talmi and I. Unna, Annu. Rev. Nucl. Sci. 10, 353 (1960).
[46]E. Bergmann, P. Bopp, Ch. Dorsch, J. Kowalsky, F. Träger, and G. zu Putlitz, Z. Phys. A 294, 319 (1980).
[47]P. Brix and H. Kopfermann, Z. Phys. 126, 344 (1949).
[48]D. N. Stacey, Rep. Prog. Phys. 29, 171 (1966).
[49]P. G. Reinhard and D. Drechsel, Z. Phys. A 290, 85 (1979).
[50]B. S. Reehal and R. A. Sorensen, Nucl. Phys. A161, 385 (1971).
[51]J. W. Negele, *Invited Papers of the Second Nuclear Physics Division Conference of the European Physics Society, 1976,* edited by A. Budzanowski and A. Kapuścik (Jagellonian University, Cracow, 1976); and Massachusetts Institute of Technology, 1978 (private communication).
[52]M. Beiner, H. Flocard, Nguyen van Giai, and P. Quentin, Nucl. Phys. A238, 29 (1975).
[53]A. Faessler, S. Krewald, A. Plastino, and J. Speth, Z. Phys. A 276, 91 (1976).
[54]A. Bouyssy and N. Vin Mau, Nucl. Phys. A229, 1 (1974).
[55]D. Gogny, Lect. Notes Phys. 108, 65 (1978).
[56]I. Sick, J. B. Bellicard, J. M. Cavedon, B. Frois, M. Huet, P. Leconte, P. X. Ho, and S. Platchkov, Phys. Lett. B88, 245 (1979).
[57]B. A. Brown, S. E. Massen, and P. E. Hodgson, J. Phys. G 12, 1655 (1979).
[58]Reinhard and Drechsel have also included octupole correlations in their calculation of the Ca isotope shifts. Because of the uncertainties concerning the collectivity of the 3^- states of these isotopes, we have not included the octupole contribution in Fig. 11.